Medical Engineering and Physics 85 (2020) 7–15

Contents lists available at ScienceDirect

Medical Engineering and Physics

journal homepage: www.elsevier.com/locate/medengphy

A low-cost scalable 3D-printed sample-holder for agitation-based decellularization of biological tissues

Dario Carbonaro[a,b], Giovanni Putame[a,b], Clotilde Castaldo[c], Franca Di Meglio[c], Katia Siciliano[a,b], Immacolata Belviso[c], Veronica Romano[c], Anna Maria Sacco[c], Fabrizio Schonauer[c], Stefania Montagnani[c], Alberto L. Audenino[a,b], Umberto Morbiducci[a,b], Diego Gallo[a,b], Diana Massai[a,b,*]

[a] Polito[BIO]Med Lab, Department of Mechanical and Aerospace Engineering, Politecnico di Torino, Turin, Italy
[b] Interuniversity Center for the Promotion of the 3Rs Principles in Teaching and Research, Italy
[c] Department of Public Health, University of Naples Federico II, Naples, Italy

ARTICLE INFO

Article history:
Received 15 March 2020
Revised 31 July 2020
Accepted 12 September 2020

Keywords:
Decellularization
Agitation
Convective flow
Biological tissues
3D printing
Computational fluid dynamics
Human skin

ABSTRACT

Decellularized extracellular matrix is one of the most promising biological scaffold supporting *in vitro* tissue growth and *in vivo* tissue regeneration in both preclinical research and clinical practice. In case of thick tissues or even organs, conventional static decellularization methods based on chemical or enzymatic treatments are not effective in removing the native cellular material without affecting the extracellular matrix. To overcome this limitation, dynamic decellularization methods, mostly based on perfusion and agitation, have been proposed. In this study, we developed a low-cost scalable 3D-printed sample-holder for agitation-based decellularization purposes, designed for treating multiple specimens simultaneously and for improving efficiency, homogeneity and reproducibility of the decellularization treatment with respect to conventional agitation-based approaches. In detail, the proposed sample-holder is able to house up to four specimens and, immersed in the decellularizing solution within a beaker placed on a magnetic stirrer, to expose them to convective flow, enhancing the solution transport through the specimens while protecting them. Computational fluid dynamics analyses were performed to investigate the fluid phenomena establishing within the beaker and to support the sample-holder design. Exploratory biological tests performed on human skin specimens demonstrated that the sample-holder reduces process duration and increases treatment homogeneity and reproducibility.

1. Introduction

In tissue engineering and regenerative medicine strategies, decellularized extracellular matrix (ECM) was demonstrated to be a promising biological scaffold to support *in vitro* tissue growth and *in vivo* tissue regeneration in both preclinical research and clinical practice [1-3]. The reasons for this are the native biochemical and biomechanical properties and the three-dimensional (3D) ultrastructure of the ECM, which provides fundamental cues for cell migration, proliferation, and differentiation [4]. Thus, to be effective, decellularization methods should remove the immunogenic cellular material of the native tissue while preserving as much as possible the ECM composition and architecture [5].

The most widely applied decellularization methods are based on static treatments with different chemical or enzymatic agents, depending on the tissue to be treated [6]. However, in case of thick tissues or even organs, static immersion in decellularizing solution could not guarantee complete decellularization, since simple molecular diffusion could not be sufficient to reach complex 3D structures deep inside [7]. Moreover, long treatment duration could affect the ECM composition and integrity, ultimately turning into a failure. For these reasons, dynamic decellularization approaches based on combined chemical/enzymatic and mechanical methods were developed. Mostly based on convective flow generated to promote the transport of the decellularization solution through the specimens, dynamic methods lead to faster and more efficient bioprocesses than static methods [8,9]. Currently, the most commonly adopted dynamic decellularization techniques are based on perfusion and agitation [10]. In perfusion-based decellularization processes, the specimen is housed within a sealed chamber

* Corresponding author.
E-mail address: diana.massai@polito.it (D. Massai).

https://doi.org/10.1016/j.medengphy.2020.09.006
1350-4533/

connected to a perfusion circuit, designed to pump and force the decellularizing solution to pass through the tissue/organ, reaching its deepest regions [11]. The perfusion-based approach is generally preferred in case of decellularization of organs, whose native vasculature is exploited to deliver treatment agents to cells and to remove cellular material from the tissue [12]. In these systems, a monitoring and control unit is usually needed since perfusion pressure has to be strictly monitored and controlled to preserve the integrity of the tissue, particularly in case of soft tissues [13]. Several studies have proved that perfusion-based methods guarantee efficient and reproducible decellularization processes [14-18], however, they are usually not conceived to treat multiple specimens simultaneously, and they require dedicated and space-consuming laboratory equipment, making the procedure complex and expensive.

Contrarily, dynamic decellularization methods based on agitation are extremely easy, cost-efficient, and performable with conventional laboratory equipment. Usually, specimens are immersed in decellularization solution, where they can freely float while being subjected to agitation, typically obtained using a magnetic stirrer, a vortex shaper or a centrifuge. Protocols adopting this method have been defined for soft and rigid tissues [19-29]. Agitation allows treating several specimens at once, however specimens are subjected to heterogeneous flow fields within the containers, where they can experience detrimental shear stresses and collisions. Moreover, when soft tissues are treated using magnetic stirrers, specimens could be entrapped around the magnetic bar, with consequent tissue damage. Although this last drawback could be overcome by enclosing the specimens in embedding cassettes, the random suspension of free-floating or embedded-in-cassette specimens causes inhomogeneous and uncontrolled transport of the decellularization solution, ultimately leading to low reproducibility of the decellularization process.

In this study, we present a novel, low-cost, scalable sample-holder for agitation-based decellularization of multiple specimens. The sample-holder was designed to be easy to use with conventional laboratory equipment, with the ultimate goal of increasing time and cost efficiency, homogeneity and reproducibility of the decellularization process. Briefly, the sample-holder, loaded with the specimens and immersed in the decellularizing solution within a beaker placed on a magnetic stirrer, exposes up to four specimens to convective flow while protecting them from disruptive forces generating within the beaker, avoiding specimen damage, reducing process duration and increasing treatment homogeneity. Computational fluid dynamics (CFD) was applied to identify the fluid phenomena establishing within the beaker and to elucidate their role in the decellularization process, and finally to support the design of the device. Proof of concept biological tests were performed on human skin specimens to demonstrate the sample-holder performance in terms of decellularization effectiveness. This latter was analyzed in terms of presence of cells, tissue architecture preservation, and collagen retention.

2. Materials and methods

2.1. Design requirements

The sample-holder design was guided by the following specific requirements: ease of use, versatility, low manufacturing cost, and need to improve process reproducibility and efficiency. More specifically, the sample-holder should be easy to assemble, handle and use with standard equipment of a cell culture laboratory. Versatility and low-cost manufacturing requirements came from the need to use the device for processing tissues of different type and size, thus it should be based on customizable and scalable design solutions, manufacturable by cost-efficient techniques. Lastly, the design of the sample-holder should guarantee to perform more efficient and reproducible decellularization processes with respect to current agitation-based techniques.

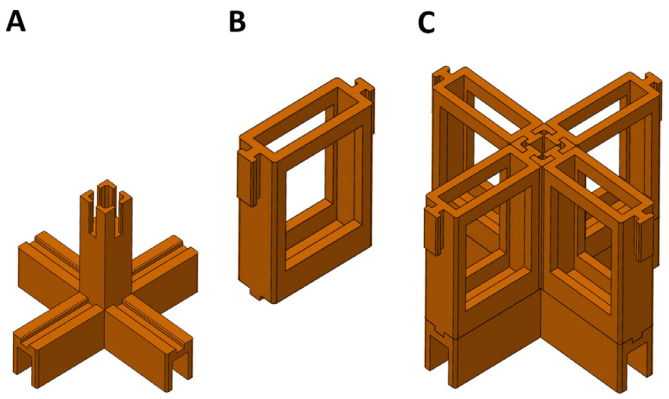

Fig. 1. 3D CAD model of the sample-holder components. (A) Cross-shaped base with central shaft. (B) Rectangular frame with T-shaped flanges. (C) Assembled sample-holder.

2.2. Design and manufacturing

Taking into account the specified requirements, the sample-holder was designed using the computer aided design (CAD) software Solidworks (Dassault Systemes, Vélizy-Villacoublay, France). For in-house rapid, flexible, and low-cost manufacturing of the sample-holder prototype, a fused deposition modeling (FDM) 3D printer (uPrint SE Plus, Stratasys, Eden Prairie, MN, USA) was used. The sample-holder components were printed in ABS plus-P430 thermoplastic material (Stratasys), used in combination with the SR30 soluble support material (Stratasys) and suitable to manufacture functional prototypes [30,31]. For guaranteeing the maximum degree of manufacturing precision, all components were printed by setting the minimum layer thickness (0.254 mm), the solid fill option, and the smart support strategy. The printing directions were defined separately for each component to minimize the consumption of support material and the working time.

2.3. Sample-holder components and use

The sample-holder is composed of a cross-shaped base with a central shaft (Fig. 1A) and four removable rectangular frames (Fig. 1B), designed to house commercial embedding cassettes, with an overall size of 91 mm x 91 mm x 67 mm. In the upper part of each rectangular frame, two T-shaped flanges allow to hook the frames to the base shaft bi-directionally (Fig. 1C). The functioning principle of the sample-holder is based on the continuous rotation of the device, immersed in the decellularizing solution, within a beaker placed on a magnetic stirrer, with the final aim to expose to a controlled convective flow the tissue specimens housed in the embedding cassettes. Fig. 2 shows step-by-step the sample-holder assembling procedure for agitation-based decellularization. Firstly, each tissue specimen is loaded in one embedding cassette, to be inserted into one frame. Then, each frame is hooked to the base (Fig. 2A), where a standard magnetic bar is inserted press-fit in the bottom (Fig. 2B). The loaded sample-holder is then positioned within a 1000 mL beaker filled with decellularizing solution and placed on a magnetic stirrer, whose rotational velocity is gradually increased up to the required value with consequent rotation of the sample-holder. During the process, the frames containing the cassettes can be removed and rotated by 180° around their longitudinal axis to expose the specimens to the same flow fields along the treatment, as described in the Results section.

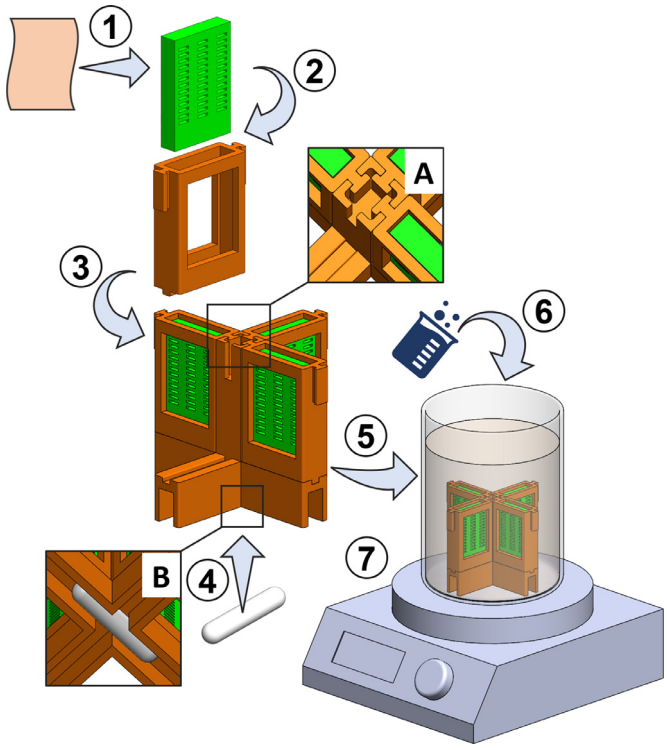

Fig. 2. Sample-holder assembling procedure for agitation-based decellularization. The step-by-step procedure consists of: 1) enclosing each specimen within one embedding cassette; 2) inserting each embedding cassette in one frame; 3) hooking the frames to the central shaft; 4) inserting press-fit the magnetic bar in the base bottom; 5) positioning the loaded sample-holder within the beaker placed on a magnetic stirrer; 6) filling the beaker with decellularizing solution; 7) switching on the magnetic stirrer, setting the required rotational velocity. (A) Detail of the coupling between the T-shaped flanges of the frames and the central shaft of the base. (B) Detail of the magnetic bar inserted press-fit in the base bottom.

2.4. In-house tests

Preliminary in-house tests were performed to assess the correct coupling of the 3D-printed components and subsequently the operational performance of the sample-holder prototype. In particular, the coupling between the frames and the cross-shaped base was checked in terms of ease of assembling and stability. Moreover, the suitability of each frame to house a commercial embedding cassette and of the base to accommodate a magnetic bar was tested. The assembled device was then housed within a 1000 mL beaker, filled with distilled water, and placed on a magnetic stirrer, whose rotational velocity was gradually increased for assessing the sample-holder prototype performance and the maximum rotational velocity value that still guarantees stability.

2.5. CFD analysis

CFD simulations were performed to investigate the fluid environment within the beaker and the action exerted by fluid forces within the specimens. Indications from the CFD analysis were used to support the sample-holder design and the definition of the operating conditions for the sample-holder decellularization process. Technically, a bidimensional section along the z-axis of the 3D model of the central shaft, the four rectangular frames, and the specimens was designed using the software Solidworks (Dassault Systemes). Based on in-house preliminary tests, three different rotational velocities of the sample-holder, i.e., 50, 100 and 150 rpm, were simulated adopting time-step integration values equal to 1.2, 0.6 and 0.4 ms, respectively. Consistently with previous works [32,33] and in order to determine the onset of a turbulent flow regime, the Reynolds number for the bulk flow within the beaker was evaluated identifying the length of the stir element (given by the sum of the length of the central shaft and two times the length of the frame in the considered bidimensional section) as the characteristic length L_s, with the velocity scale identification based on the rotational velocity N (in revolutions per second) multiplied for L_s, as it follows:

$$Re = \frac{N L_s^2}{\nu_m} \tag{1}$$

where ν_m is the kinematic viscosity of the culture medium, defined as the ratio of the dynamic viscosity to the density. The Reynolds numbers characterizing the fluid dynamics in the bulk of the proposed set up were equal to 6880 (at 50 rpm), 13,760 (at 100 rpm), and 20,640 (at 150 rpm). The geometry was discretized with the meshing toolbox of Workbench (Ansys Inc., Canonsburg, PA, USA) by using approximately 280 $\times$ 10^3 triangular elements. The governing equations of motion were solved, in their discretized form, by using the commercial finite-volume software FLUENT (Ansys Inc). The rigid-body rotation of the sample-holder, responsible for setting in motion the decellularization solution, was prescribed by using a rotating reference frame, while stationary wall and no-slip conditions were imposed for the beaker. A dynamic remeshing based on local cell skewness value was adopted for the fluid zone corresponding to the decellularizing solution. Reynolds-averaged Navier-Stokes (RANS) equations with RNG k-ε turbulence model [34] were solved assuming the decellularizing solution as an incompressible Newtonian fluid, and a source term S was added to simulate the flow through the specimens, modeled as porous media:

$$\begin{aligned} &\nabla \cdot \bar{\boldsymbol{u}} = 0 \\ &\rho \tfrac{D\bar{\boldsymbol{u}}}{Dt} = -\nabla \bar{p} - \left[\nabla \cdot \bar{\tau}^{(l)}\right] - \left[\nabla \cdot \bar{\tau}^{(t)}\right] + \rho g + S \end{aligned} \tag{2}$$

where $\boldsymbol{u}$ is the velocity vector, $\boldsymbol{g}$ is the gravitational acceleration, ρ is the fluid density (10^3 kg/m^3), p is the pressure, τ is the shear stress tensor decomposed in its laminar (i.e., viscous) and turbulent components ($\tau^{(l)}$ and $\tau^{(t)}$, respectively), and the overbar denotes a time-averaged quantity. The source term S implemented the Forchheimer equation, which defines pressure losses through the porous medium as a sum of viscous losses, predominant in case of laminar flow, and inertial losses, predominant in case of turbulent flow:

$$S = -\left(\frac{\mu}{k}(\bar{\boldsymbol{u}} - \boldsymbol{\omega} \times \boldsymbol{r}) + C_2 \frac{1}{2}\rho|\bar{\boldsymbol{u}} - \boldsymbol{\omega} \times \boldsymbol{r}|(\bar{\boldsymbol{u}} - \boldsymbol{\omega} \times \boldsymbol{r})\right) \tag{3}$$

where μ is the dynamic viscosity of the fluid (1.003×10^{-3} kg/(m•s)), $\boldsymbol{\omega}$ is the rotational velocity of the sample-holder, $\boldsymbol{r}$ is the radial distance of the fluid element from the center of rotation, $1/k$ and C_2 are the viscous resistance coefficient and the inertial resistance coefficient of the specimens, respectively [35]. For the specimens, the permeability parameters were set according to the work of Israelowitz and colleagues on porous scaffolds [36], reported in Table 1.

Table 1
Imposed porous medium parameters.

Parameter	Value
Viscous resistance coefficient, $1/k$	$2 \bullet 10^8$ m^{-2}
Inertial resistance coefficient, C_2	5648 m^{-1}
Porosity	0.8

For each modeled angular velocity, three sample-holder revolutions were simulated. The flow field was evaluated in terms of velocity and static pressure distributions. The mechanical action exerted by the decellularizing solution flowing within the specimens was quantified also in terms of viscous shear stress $\bar{\tau}^{(l)}$ and

turbulent shear stress $\bar{\tau}^{(t)}$. Technically, turbulent shear stress was evaluated in terms of maximum turbulent shear stress (TSS_{max}), calculated starting from the two principal stresses σ_1 and σ_2 of the stress tensor $\bar{\tau}^{(t)}$ as it follows:

$$TSS_{\max} = \frac{1}{2}(\sigma_1 - \sigma_2) \quad (4)$$

Further details on the calculation of viscous shear stresses and the TSS_{max} are provided in the Supplementary Material.

2.6. Exploratory biological tests

2.6.1. Tissue specimens and decellularization procedure

Human adult skin samples were obtained from patients undergoing plastic surgery ($n = 4$, mean age 34 ± 1.15). Upon receipt, samples were washed, hairs and adipose tissue were removed, and multiple specimens from each patient were scaled down to fit within commercial embedding cassettes (length = 30 mm, width = 25 mm, thickness = 5 mm).

Based on a recently described protocol [28,29], a decellularization solution containing 1% w/v sodium dodecyl sulfate (SDS), 1% v/v Triton, and a combination of antibiotics (0.25 μg/ml Amphotericin B, 100 U/ml Penicillin, 50 U/ml Streptomycin) was used. All skin specimens were enclosed into embedding cassettes, in order to protect them, and then treated with or without the sample-holder under constant agitation, using a 1000 mL beaker filled with 700 mL of decellularization solution and placed on a magnetic stirrer (rotational velocity = 150 rpm). In detail, the first subset of cassettes was immersed directly in the decellularizing solution within the beaker, free to float in agitation, and indicated as the free-floating cassette (FFC) group. The second subset of cassettes was inserted in the sample-holder within the beaker and kept that way for the entire duration of the agitation-based decellularization process, thus indicated as the sample-holder cassette (SHC) group. The third subset of cassettes was inserted in the sample-holder within the beaker and, after 12 h of treatment in agitation, the frames housing the cassettes were rotated by 180° around their longitudinal axis, so indicated as the rotated sample-holder cassette (RSHC) group. The decellularization procedure was considered complete when the specimens became thoroughly white. This occurred after 24 h in specimens treated using the sample-holder, and after 36 h in specimens treated using free-floating cassettes. However, for comparing FFC, SHC and RSHC groups, specimens from FFC group were harvested also after 24 h of decellularization. Hence, after 24 or 36 h of treatment, all specimens were rinsed for 24 h in antibiotic solution and for additional 30 min in sterile bi-distilled water. In addition, each SHC specimen was then sectioned along its longitudinal axis into two halves, one proximal and one distal to the sample-holder shaft, respectively. Samples were processed for histological analysis, or snap frozen at −80 °C for collagen quantitative assay.

2.6.2. Histochemistry

Treated specimens were fixed in 10% neutral-buffered formalin, dehydrated in a graded series of alcohols, cleared in xylene, and infiltrated and embedded in paraffin, according to standard protocols. Paraffin blocks were then sliced into serial 5-μm-thick sections and placed on poly-lysine-coated glass slides. Sections of specimens were deparaffinized, rehydrated and stained with Hematoxylin and Eosin or Masson's trichrome stainings using specific staining kits (Bio-Optica, Milan, Italy) to evaluate the effectiveness of decellularization, tissue architecture and collagen retention. Stained sections were observed by at least three independent observers using a light microscope 147 DM2000 Led (Leica Microsystems, Wetzlar, Germany) equipped with an ICC50HD camera (Leica Microsystems) for microphotography.

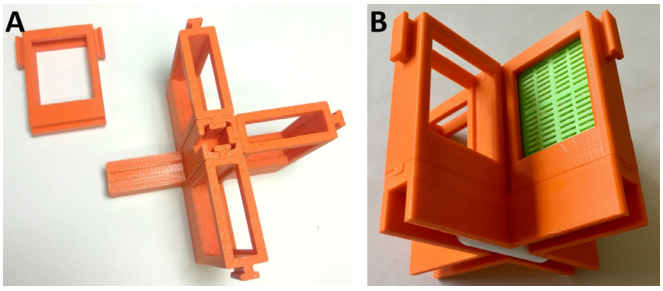

Fig. 3. 3D-printed sample-holder. (A) 3D-printed sample-holder components. (B) Sample-holder loaded with one embedding cassette and provided with the magnetic bar.

2.6.3. Collagen quantitative analysis

The evaluation of the total collagen content in treated specimens was performed by S1000/S2000 Sircol Assay (Biocolor, Ltd, Carrickfergus, UK), a colorimetric dye-binding method suitable for the quantification of soluble and insoluble collagen. In accordance with the protocol provided by the manufacturer, 20 mg of each specimen were digested in acetic acid (0.5 M in 0.1 mg/ml pepsin) at 4 °C overnight for soluble collagen extraction. The digestion was blocked by adding Acid Neutralizing Reagent (TRIS-HCl and NaOH). For insoluble collagen extraction, specimens were then incubated with Fragmentation Reagent (diluted acetic acid, antimicrobial agents and surfactants) at 65 °C in a temperature controlled water-bath for 2 h. Successively, Sircol Dye Reagent (Sirius Red in picric acid) was added to each specimen extract and incubated for 30 min on a shaker to allow the formation of a collagen-dye complex precipitate. All specimens were then centrifuged, drained and washed with Acid-Salt Wash Reagent (ice-cold acetic acid, sodium chloride and surfactants) to remove unbound dye. Collagen-dye complexes were finally dissolved in Alkali Reagent (0.5 M sodium hydroxide) on a vortex to allow the release of Sircol dye from the complexes before proceeding with absorbance reading. Each specimen was transferred to individual wells of a 96-well plate. The absorbance was read in an ELx800 Absorbance Microplate Reader (BioTek Instruments, Winooski, VT, USA) and analyzed with Microsoft Excel (Microsoft Corp, Redmond, WA, USA) to generate the calibration curve and calculate the final concentration of total collagen for each absorbance reading.

2.6.4. Statistical analysis

Statistical analysis was performed using GraphPad Prism version 5.00 for Windows (GraphPad Software, San Diego, CA, USA). Measurements were performed in triplicate for each sample ($n = 4$) and data were expressed as the mean ± standard error of the mean and analyzed using Kruskal-Wallis nonparametric test. A value of $p \leq 0.05$ was used to identify any statistically significant differences.

3. Results

3.1. In-house tests

The correct coupling and ease of assembling of the components of the sample-holder prototype were confirmed (Fig. 3A), along with the suitability of both the frames to house the embedding cassettes and the base to accommodate the magnetic bar (Fig. 3B). Tests performed with the assembled device put within a beaker, filled with distilled water and placed on a magnetic stirrer showed that the sample-holder starts to rotate when a rotational velocity of 50 rpm is imposed, and continues to rotate stably up to 160 rpm, with its rotating axis centered with the beaker and no component detachment. For higher rotational velocity values, the

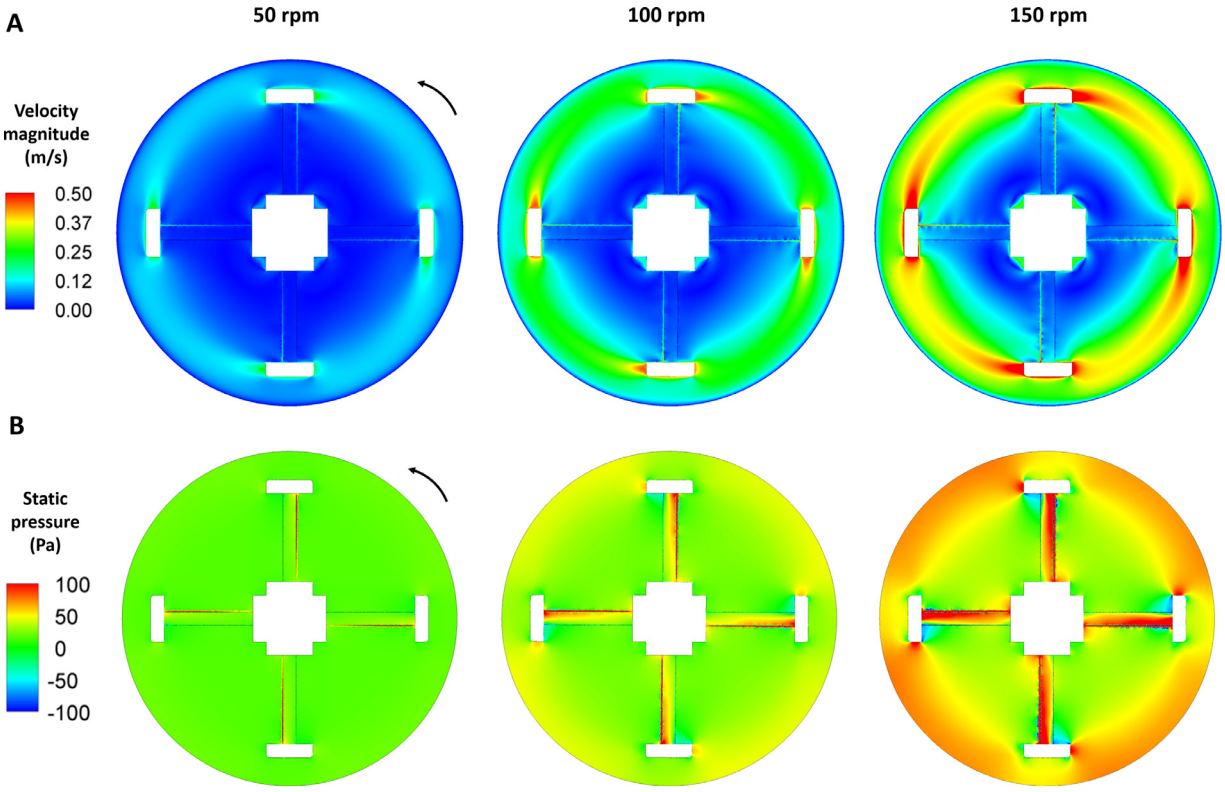

Fig. 4. Computational velocity magnitude (A) and static pressure (B) distributions at the end of the third revolution imposing sample-holder rotational velocity values of 50, 100 and 150 rpm.

sample-holder starts to fluctuate unstably within the beaker (see Supplementary Movie 1). This test confirmed the sample-holder prototype performance and the ease of use with conventional laboratory equipment. The 3D printing procedure took a global working time of about 12 h.

3.2. CFD analysis

For all the simulated rotational velocities, the animations of the velocity magnitude and static pressure distributions within the beaker showed that the initial transient lasts less than one revolution of the sample-holder (see Supplementary Movie 2). In detail, the contour maps of the fluid velocity magnitude distribution within the beaker at the three simulated rotational velocities (50, 100, and 150 rpm) highlighted that, as the rotational velocity increases, the fluid velocity through the specimens increases as well, maintaining similar relative spatial distributions (Fig. 4A). Concerning the static pressure contour maps, it emerged that increasing the rotational velocity, the static pressure within each specimen increases, presenting a not uniform distribution within the specimens (Fig. 4B). This interestingly suggested a “penetration profile” for the decellularizing solution from the rear side of the specimens which increases radially almost linearly starting from the center of rotation, with higher static pressure values in the distal parts of the specimens than in the proximal ones (Fig. 4B). Viscous shear stresses (Fig. 5A) and TSS_{max} (Fig. 5B) within the specimens presented similar distributions as the static pressure, with viscous shear stress values at least two orders of magnitude smaller than TSS_{max} values.

3.3. Exploratory biological tests

Exploratory biological tests were performed on human skin samples treated under different conditions for evaluating the sample-holder performance for agitation-based decellularization. Recapitulating, all specimens were enclosed in embedding cassettes and treated under agitation (150 rpm). The FFC group consisted of cassettes immersed directly in the decellularizing solution within the beaker, free to float in agitation, and treated for 24 or 36 h. The SHC group was composed of cassettes inserted in the sample-holder within the beaker and kept that way for the entire duration of the decellularization process (24 h). Inspired by the CFD outcomes, the RSHC group comprised cassettes inserted in the sample-holder within the beaker and, after 12 h, rotated with their frames by 180° around their longitudinal axis, for a total treatment duration of 24 h. Specimens of SHC and RSHC groups became thoroughly white after 24 h, while FFC specimens needed 36 h. Decellularization effectiveness in terms of presence of cell nuclei and tissue architecture preservation was assessed by Hematoxylin and Eosin staining and compared with native skin (Fig. 6A). After 24 h of treatment, cell nuclei were still observable in the inner dermis of FFC specimens (Fig. 6B), and additional 12 h of treatment were necessary to achieve their thorough decellularization (Fig. 6D). Differently, the absence of epidermal stratified epithelium and dermal cell nuclei resulted evident in specimens treated using the sample-holder already after 24 h of treatment (Fig. 6C RSHC group, and Figs. 6E and 6F SHC group). Comparing completely decellularized specimens, although only slight differences emerged from a macroscopic examination, the histological analysis highlighted a better preserved tissue architecture in specimens treated using the sample-holder (Figs. 6C, 6E, and 6F) than in FFC specimens (Fig. 6D). Notably, in SHC specimens the part distal to the sample-holder shaft (Fig. 6F), exposed to higher static pressure and shear stress values, presented a less preserved tissue architecture with respect to the proximal one (Fig. 6E).

To evaluate the effects of the decellularization procedure on the retention and distribution of collagen in treated specimens, the Masson’s trichrome staining and the quantitative dye-binding assay

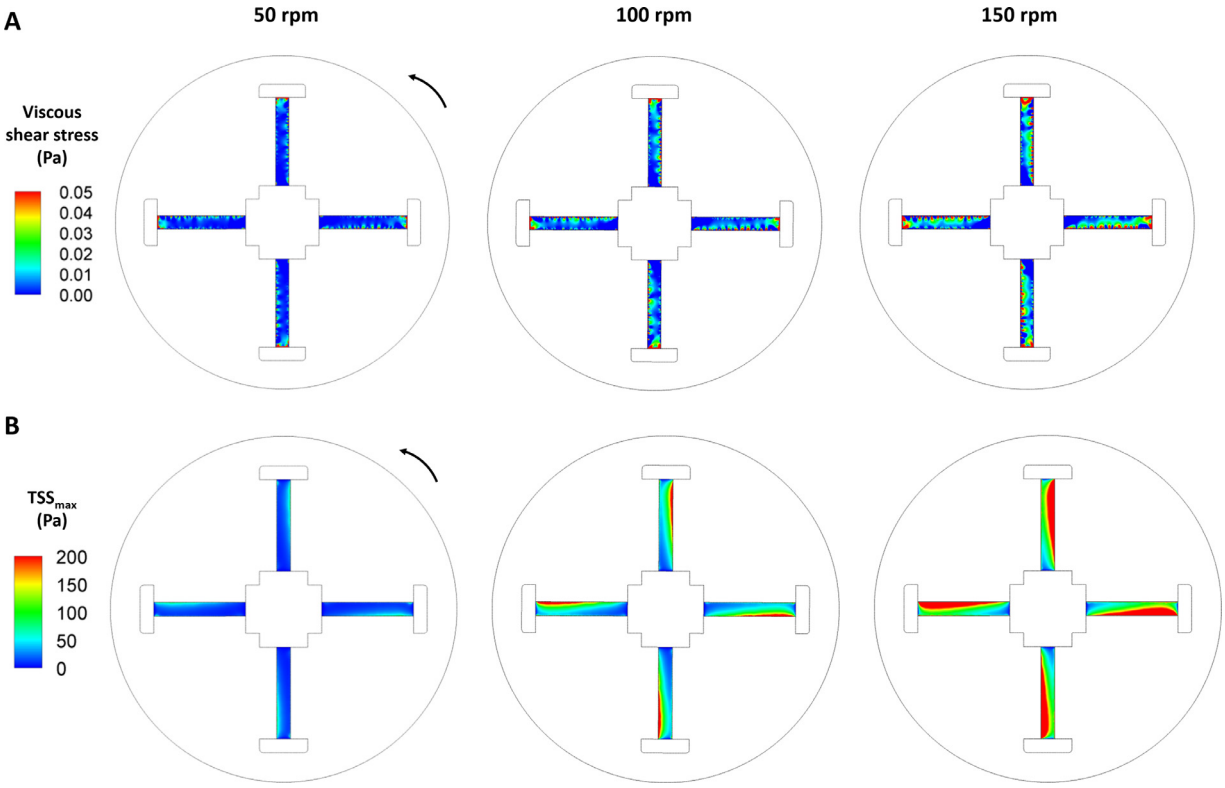

Fig. 5. Computational viscous shear stress (A) and maximum turbulent shear stress (B) distributions within the specimens imposing sample-holder rotational velocity values of 50, 100 and 150 rpm.

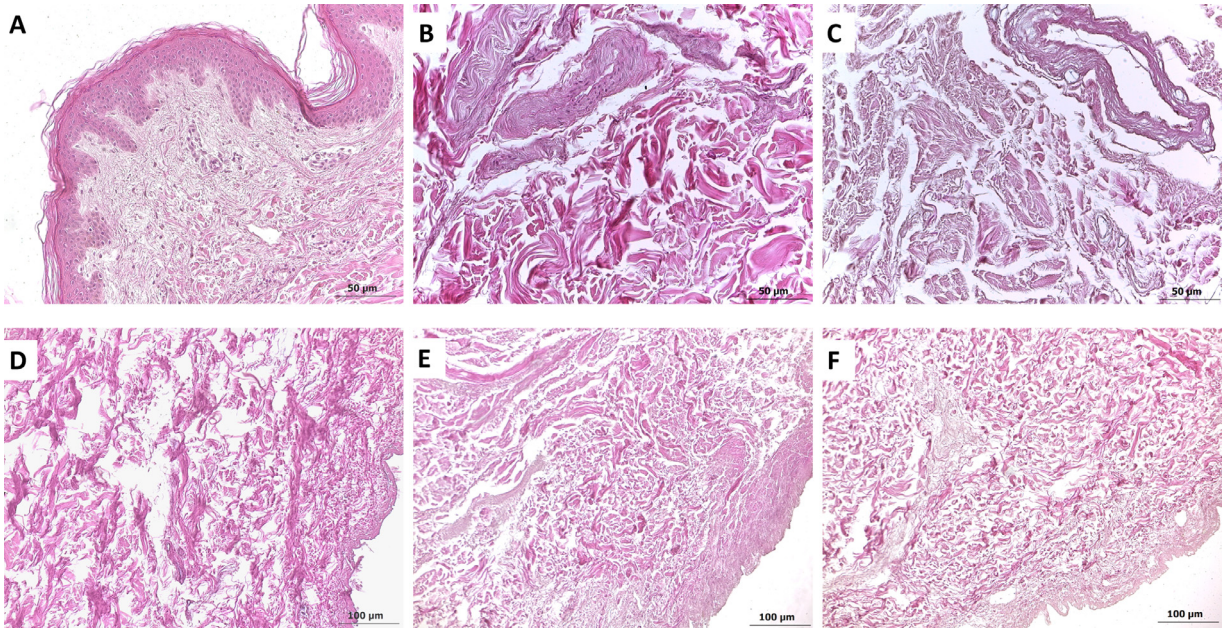

Fig. 6. Representative images of hematoxylin and eosin staining of native skin (A) and treated specimens (B-F) for the evaluation of the effectiveness of the decellularization procedure and tissue architecture after 24 h (B, C, E, and F) or 36 h (D) of treatment. After 24 h of decellularization treatment, inner dermal cells were still visible in FFC specimens (B), while RSHC specimens (C) and the proximal (E) and distal (F) parts of the SHC specimens resulted thoroughly acellular and well preserved in their architecture. Specimens decellularized using the sample-holder (C, E, and F) showed a better preserved organization of the dermal connective tissue than FFC specimens (D). A-C scale bar = 50 μm; D-F scale bar = 100 μm.

were performed. Histological analysis showed collagen retention in both FFC specimens treated for 36 h and in SHC and RSHC groups treated for 24 h (Fig. 7). However, the collagen network in RSHC specimens (Fig. 7B) was observed to be slightly better preserved than the network of the distal parts of the SHC group (Fig. 7D). Although the quantitative dye-binding assay highlighted that FFC specimens retained higher amounts of collagen than RSHC and SHC specimens (14.09 $\pm$ 2.05 vs 12.22 $\pm$ 1.93 vs 10.22 $\pm$ 1.29 μg/mg dry tissue, respectively, Fig. 8), the observed difference was not significant ($p = 0.36$).

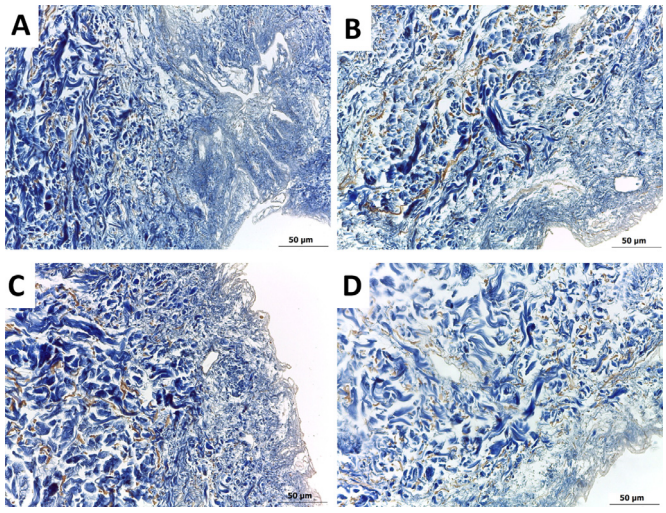

Fig. 7. Representative images of Masson's trichrome staining for the evaluation of collagen presence and distribution after 36 h (A) or 24 h (B-D) of treatment. Collagen fibers (blue color) were retained in FFC specimens (A), RSHC specimens (B), and in the proximal (C) and distal (D) parts of SHC specimens. However, in SHC specimens an uneven preservation of collagen network emerged, as testified by the darker blue color in the proximal half (C) of SHC specimens with respect to the distal one (D). Scale bar = 50 μm.

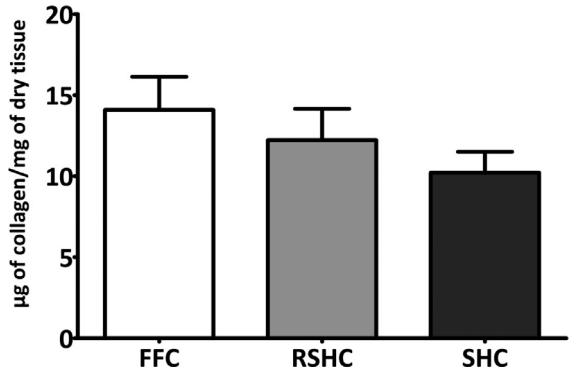

Fig. 8. Quantification of collagen by specific dye-binding assay. No statistically significant difference emerged from the comparison of FFC, RSHC and SHC specimens.

4. Discussion

In native tissues, ECM is a crucial and active modulator of cell behavior. Its biological and physical signals and complex 3D ultrastructure form together a dynamic environment that regulates the survival, proliferation, migration, and differentiation of resident cells [37]. Because of the challenges associated with preparing synthetic materials recapitulating the entirety of ECM extrinsic signals, significant efforts have been dedicated to develop efficient and reliable methods for extracting the native ECM from biological tissues without adversely affecting its biochemical and biomechanical properties [9]. In particular, a number of decellularization procedures based on chemical, enzymatic and/or physical methods have been proposed with the ultimate goal of removing all the antigenic epitopes associated with cell membranes and intracellular components, while preserving ECM composition and architecture [38,39].

Decellularized ECM has been successfully adopted as biological scaffold to regenerate several tissues and organs, and recently interest is increasing for human tissue grafts obtained by repopulating decellularized scaffolds with patient's own cells or human pluripotent stem cells [9,14,39-42]. In the perspective of clinical applications, it becomes essential to translate highly specialized protocols to reproducible and scalable bio-processes [43]. In this effort towards process standardization, we developed a low-cost scalable sample-holder for agitation-based decellularization, designed for treating multiple specimens simultaneously and for increasing the homogeneity, reproducibility, and efficiency of the decellularization process with respect to conventional agitation-based approaches. The sample-holder was designed, 3D-printed, and characterized adopting advanced engineering methods and computational and experimental approaches. The use of the CAD software streamlined the design phase and allowed modifying and scaling easily the final geometry, and the adopted 3D printing technology enabled to produce the device in-house, providing strict design-to-prototype timing, customization flexibility, and time and cost effective rapid-prototyping. Preliminary tests performed in-house demonstrated the ease of assembling of the sample-holder prototype components, and the ease of use and correct operational functioning of the device with conventional lab equipment. In detail, the sample-holder, loaded with the specimens and immersed in the decellularizing solution within a beaker placed on a magnetic stirrer, can rotate stably for rotational velocity values ranging from 50 to 160 rpm (Supplementary Movie 1), allowing to be used in several operating conditions. Moreover, its modular structure permits to treat up to four specimens simultaneously while managing each specimen independently. The customizable and scalable design makes the sample-holder versatile and suitable to be adapted to specimens of different types and sizes.

The CFD approach was a valuable tool not only for providing a comprehensive analysis/identification of the physical phenomena establishing within the beaker in presence of the sample-holder in agitation, but also for supporting the sample-holder design, allowing to go beyond the common time and cost consuming experimental trial-and-error approach [44-48]. CFD simulations were carried out imposing three rotational velocities (50, 100, and 150 rpm). As expected, when the imposed rotational velocity was increased, the fluid velocity, the static pressure, and the viscous and turbulent shear stress values through the specimens increased as well (Figs. 4 and 5). CFD simulations showed that increasing the imparted rotational velocity the front and rear sides and the proximal and distal parts of each specimen are exposed to markedly different values of static pressure and shear stress (Figs. 4 and 5). This suggests that the decellularizing solution is characterized by a "penetration profile" that increases radially within the specimens and could exert a not uniform mechanical action on them, leading to inhomogeneous decellularization treatment. Moreover, high static pressure and shear stress values can promote and speed up the decellularization process, but at the same time they could affect the architecture of the tissue. These observations inspired the design of the bidirectionally hookable frames, whose appropriate cyclic rotation exposes all parts of the specimens to the same flow fields along the treatment, ultimately increasing the process homogeneity.

This was confirmed by the exploratory biological tests carried out to assess the performance of the sample-holder in terms of decellularization effectiveness. In detail, human skin specimens were enclosed in embedding cassettes to protect them, and then they were treated under agitation in different conditions. A rotational velocity of 150 rpm was imposed for all experiments, inspired by in-house tests and computational outcomes. Above all, the use of the sample-holder allowed reducing the treatment duration, indeed RSHC and SHC groups reached a complete decellularization already after 24 h (Figs. 6C, 6E and 6F), while the FFC group needed 36 h (Fig. 6D). The better preserved tissue architecture observed in RSHC (Fig. 6C) and SHC specimens (Figs. 6E and 6F) compared to decellularized FFC specimens (Fig. 6D) confirms that the use of the sample-holder, by reducing the treatment duration, improves the preservation of the ECM architecture. As concerns the retained collagen content, all groups showed colla-

gen retention (Fig. 7), with no statistically significant differences (Fig. 8). Noteworthy, observing the SHC specimens, the parts distal to the sample-holder shaft were characterized by less preserved tissue architecture (Fig. 6F) and collagen network (Fig. 7D) with respect to the proximal ones (Fig. 6E and Fig. 7C, respectively). This result, combined with the computational outcomes, indicates that the higher static pressure and TSS_{max} values experienced by the distal parts of the specimens compared to the proximal parts overall cause an inhomogeneous treatment of the specimens, which can be avoided rotating the frames cyclically.

The biological findings, in accordance with the CFD analysis, demonstrated that the use of the sample-holder exposes the specimens to defined convective flow, which promotes the transport of the decellularizing solution through them, leading to faster and more reproducible decellularization processes. Moreover, the cyclic rotation of the frames increases the treatment homogeneity, and consequently the decellularization quality.

Some limitations could affect this study. For cleaning procedure, the here adopted 3D printing material is not autoclavable, however the sample-holder is at a prototypal stage and in the future different manufacturing technologies and materials will be accounted for large-scale production, taking into account both the biocompatibility and the manufacturing process requirements [49,50]. Concerning the CFD analysis, several assumptions were made. Specimens were assumed as rigid bodies, while in reality they are soft and easily deformable tissues. However, being enclosed in embedding cassettes, the latter served as structural and protecting support reducing the specimen deformation. Moreover, as concerns the porous medium parameters adopted, values typical of rigid scaffolds were assumed since we couldn't find in literature data on viscous and inertial resistance coefficients for human skin tissue. In addition, it should be considered that, along the decellularization process, the permeability of the specimens should increase. In order to overcome these limitations, future studies will account for permeability values calculated experimentally for the specific treated tissues at different time points during the process [51,52]. Lastly, although the adopted RNG k-ε turbulence modeling is tailored for isotropic turbulence, it allowed reducing the computational effort and was sufficiently accurate for describing flows involving rotation and high strain rates [53]. In the future, the computational approach could be integrated with an advection-diffusion-reaction model for characterizing in-depth the decellularizing agent transport through the specimens.

In conclusion, the sample-holder prototype met the defined design requirements of ease of use, versatility, and low-cost manufacturing, and ultimately allowed improving efficiency, reproducibility, and homogeneity of the decellularization process with respect to conventional agitation-based approaches. Being scalable and designed for transport-based processes, the proposed device could be used also for tissue fixation, scaffold functionalization or scaffold drug loading, supporting widespread accessibility and use in research, industry, and clinics.

Funding

None.

Ethical approval

Patients provided written informed consent and samples were collected without patient identifiers, following protocols approved by the Federico II University Hospital Ethical Committee (ref. number 79/18) and in conformity with principles outlined in the Declaration of Helsinki.

Declaration of Competing Interests

None declared. The sample-holder is currently patent pending.

Supplementary materials

Supplementary material associated with this article can be found, in the online version, at doi:10.1016/j.medengphy.2020.09.006.

References

[1] Badylak SF, Taylor D, Uygun K. Whole-organ tissue engineering: decellularization and recellularization of three-dimensional matrix scaffolds. Annu Rev Biomed Eng 2011;13:27–53 https://doi.org/. doi:10.1146/annurev-bioeng-071910-124743.
[2] Porzionato A, Stocco E, Barbon S, Grandi F, Macchi V, De Caro R. Tissue-engineered grafts from human decellularized extracellular matrices: a systematic review and future perspectives. Int J Mol Sci 2018;19:4117 https://doi.org/. doi:10.3390/ijms19124117.
[3] Zhang B, Xue Q, Li J, Ma L, Yao Y, Ye H, et al. 3D bioprinting for artificial cornea: challenges and perspectives. Med Eng Phys 2019;71:68–78 https://doi.org/. doi:10.1016/j.medengphy.2019.05.002.
[4] Crapo PM, Gilbert TW, Badylak SF. An overview of tissue and whole organ decellularization processes. Biomaterials 2011;32:3233–43 https://doi.org/. doi:10.1016/j.biomaterials.2011.01.057.
[5] Gilbert TW, Sellaro TL, Badylak SF. Decellularization of tissues and organs. Biomaterials 2006;27:3675–83 https://doi.org/. doi:10.1016/j.biomaterials.2006.02.014.
[6] Song JJ, Ott HC. Organ engineering based on decellularized matrix scaffolds. Trends Mol Med 2011;17:424–32 https://doi.org/. doi:10.1016/j.molmed.2011.03.005.
[7] Kajbafzadeh AM, Javan-Farazmand N, Monajemzadeh M, Baghayee A. Determining the optimal decellularization and sterilization protocol for preparing a tissue scaffold of a human-sized liver tissue. Tissue Eng - Part C 2013;19:642–51 https://doi.org/. doi:10.1089/ten.tec.2012.0334.
[8] Goissis G, Suzigan S, Parreira DR, Maniglia JV, Braile DM, Raymundo S. Preparation and characterization of collagen-elastin matrices from blood vessels intended as small diameter vascular grafts. Artif Organs 2000;24:217–23 https://doi.org/. doi:10.1046/j.1525-1594.2000.06537.x.https://doi.org/10.1089/ten.tec.2012.0334.
[9] Gilpin A, Yang Y. Decellularization strategies for regenerative medicine: from processing techniques to applications. Biomed Res Int 2017;2017:9831534 https://doi.org/. doi:10.1155/2017/9831534.
[10] Keane TJ, Swinehart IT, Badylak SF. Methods of tissue decellularization used for preparation of biologic scaffolds and in vivo relevance. Methods 2015;84:25–34 https://doi.org/. doi:10.1016/j.ymeth.2015.03.005.
[11] Fu RH, Wang YC, Liu SP, Shih TR, Lin HL, Chen YM, et al. Decellularization and recellularization technologies in tissue engineering. Cell Transplant 2014;23:621–30 https://doi.org/. doi:10.3727/096368914X678382.
[12] Crapo PM, Gilbert TW, Badylak SF. An overview of tissue and whole organ decellularization processes. Biomaterials 2011;32:3233–43 https://doi.org/. doi:10.1016/j.biomaterials.2011.01.057.
[13] Guyette JP, Gilpin SE, Charest JM, Tapias LF, Ren X, Ott HC. Perfusion decellularization of whole organs. Nat Protoc 2014;9:1451–68 https://doi.org/. doi:10.1038/nprot.2014.097.1016/j.biomaterials.2011.01.057.
[14] Garreta E, Oria R, Tarantino C, Pla-Roca M, Prado P, Fernández-Avilés F, et al. Tissue engineering by decellularization and 3D bioprinting. Mater Today 2017;20:166–78 https://doi.org/. doi:10.1016/j.mattod.2016.12.005.
[15] Daryabari SS, Kajbafzadeh AM, Fendereski K, Ghorbani F, Dehnavi M, Rostami M, et al. Correction to: development of an efficient perfusion-based protocol for whole-organ decellularization of the ovine uterus as a human-sized model and in vivo application of the bioscaffolds. J Assist Reprod Genet 2019;36:2191 https://doi.org/. doi:10.1007/s10815-019-01578-8.
[16] Kajbafzadeh AM, Khorramirouz R, Nabavizadeh B, Ladi Seyedian SS, Akbarzadeh A, Heidari R, et al. Whole organ sheep kidney tissue engineering and in vivo transplantation: effects of perfusion-based decellularization on vascular integrity. Mater Sci Eng C 2019;98:392–400 https://doi.org/. doi:10.1016/j.msec.2019.01.
[17] Schilling BK, Lamberti KK, Snowden MJ, Baker JS, Byrd K, Komatsu C, et al. Design and fabrication of an automatable, 3d printed perfusion device for tissue infusion and perfusion engineering. Tissue Eng Part A 2019 ten.tea.2019.0209https://doi.org/. doi:10.1089/ten.tea.2019.0209.018.
[18] Willemse J, Verstegen MMA, Vermeulen A, Schurink IJ, Roest HP, van der Laan LJW, et al. Fast, robust and effective decellularization of whole human livers using mild detergents and pressure controlled perfusion. Mater Sci Eng C 2020;108:110200 https://doi.org/. doi:10.1016/j.msec.2019.110200.
[19] Alshaikh AB, Padma AM, Dehlin M, Akouri R, Song MJ, Brännström M, et al. Decellularization of the mouse ovary: comparison of different scaffold generation protocols for future ovarian bioengineering. J Ovarian Res 2019;12:58 https://doi.org/. doi:10.1186/s13048-019-0531-3.
[20] Ferdowsi Khosroshahi A, Soleimani Rad J, Kheirjou R, Roshangar B, Rashtbar M, Salehi R, et al. Adipose tissue-derived stem cells upon decellular-

ized ovine small intestine submucosa for tissue regeneration: an optimization and comparison method. J Cell Physiol 2020;235:1556–67 https://doi.org/. doi:10.1002/jcp.29074.
[21] Montoya CV, McFetridge PS. Preparation of ex vivo based biomaterials using convective flow decellularization. Tissue Eng - Part C 2009;15:191–200 https://doi.org/. doi:10.1089/ten.tec.2008.0372.
[22] Syed O, Walters NJ, Day RM, Kim HW, Knowles JC. Evaluation of decellularization protocols for production of tubular small intestine submucosa scaffolds for use in oesophageal tissue engineering. Acta Biomater 2014;10:5043–54 https://doi.org/. doi:10.1016/j.actbio.2014.08.024.
[23] Wilson SL, Sidney LE, Dunphy SE, Dua HS, Hopkinson A. Corneal decellularization: a method of recycling unsuitable donor tissue for clinical translation? Curr Eye Res 2016;41:769–82 https://doi.org/. doi:10.3109/02713683.2015.1062114.
[24] Stern MM, Myers RL, Hammam N, Stern KA, Eberli D, Kritchevsky SB, et al. The influence of extracellular matrix derived from skeletal muscle tissue on the proliferation and differentiation of myogenic progenitor cells ex vivo. Biomaterials 2009;30:2393–9 https://doi.org/. doi:10.1016/j.biomaterials.2008.12.069.
[25] Reing JE, Brown BN, Daly KA, Freund JM, Gilbert TW, Hsiong SX, et al. The effects of processing methods upon mechanical and biologic properties of porcine dermal extracellular matrix scaffolds. Biomaterials 2010;31:8626–33 https://doi.org/. doi:10.1016/j.biomaterials.2010.07.083.
[26] Cebotari S, Tudorache I, Jaekel T, Hilfiker A, Dorfman S, Ternes W, et al. Detergent decellularization of heart valves for tissue engineering: toxicological effects of residual detergents on human endothelial cells. Artif Organs 2010;34:206–10 https://doi.org/. doi:10.1111/j.1525-1594.2009.00796.x.
[27] Crapo PM, Medberry CJ, Reing JE, Tottey S, Van der Merwe Y, Jones KE, et al. Biologic scaffolds composed of central nervous system extracellular matrix. Biomaterials 2012;33:3539–47 https://doi.org/. doi:10.1016/j.biomaterials.2012.01.044.
[28] Di Meglio F, Nurzynska D, Romano V, Miraglia R, Belviso I, Sacco AM, et al. Optimization of human myocardium decellularization method for the construction of implantable patches. Tissue Eng - Part C 2017;23:525–39 https://doi.org/. doi:10.1089/ten.tec.2017.0267.
[29] Belviso I, Romano V, Sacco AM, Ricci G, Massai D, Cammarota M, et al. Decellularized human dermal matrix as a biological scaffold for cardiac repair and regeneration. Front Bioeng Botechnol 2020 in press. https://doi.org/. doi:10.3389/fbioe.2020.00229.
[30] Putame G, Terzini M, Carbonaro D, Pisani G, Serino G, Di Meglio F, et al. Application of 3D printing technology for design and manufacturing of customized components for a mechanical stretching bioreactor. J Healthc Eng 2019;2019:3957931 https://doi.org/. doi:10.1155/2019/3957931.
[31] Putame G, Gabetti S, Carbonaro D, Di Meglio F, Romano V, Sacco AM, et al. Compact and tunable stretch bioreactor advancing tissue engineering implementation. Application to engineered cardiac constructs. Med Eng Phys 2020 https://doi.org/. doi:10.1016/j.medengphy.2020.07.018.
[32] Sucosky P, Osorio DF, Brown JB, Neitzel GP. Fluid mechanics of spinner flask bioreactor. Biotechnol Bioeng 2003;85:34–46 https://doi.org/. doi:10.1002/bit.10788.
[33] Vunjak-Novakovic G, Freed LE, Biron RJ, Langer R. Effects of mixing on the composition and morphology of tissue engineered cartilage. AIChE J 1996;42:850–60 https://doi.org/. doi:10.1002/aic.690420323.
[34] Wilcox DC. Turbulence modeling for CFD. La Canada: DCW Industries; 1998.
[35] Vafai K, Tien CL. Boundary and inertia effects on flow and heat transfer in porous media. Int J Heat Mass Transf 1981;24:195–203 https://doi.org/. doi:10.1016/0017-9310(81)90027-2.
[36] Israelowitz M, Weyand B, Rizvi S, Vogt PM, Von Schroeder HP. Development of a laminar flow bioreactor by computational fluid dynamics. J Healthc Eng 2012;3:455–76 https://doi.org/. doi:10.1260/2040-2295.3.3.455.
[37] Lockhart M, Wirrig E, Phelps A, Wessels A. Extracellular matrix and heart development. Birth Defects Res A Clin Mol Teratol 2011;91:535–50 https://doi.org/. doi:10.1002/bdra.20810.
[38] Badylak SF, Freytes DO, Gilbert TW. Extracellular matrix as a biological scaffold material: structure and function. Acta Biomater 2009;5:1–13 https://doi.org/. doi:10.1016/j.actbio.2008.09.013.
[39] Fernández-Pérez J, Ahearne M. The impact of decellularization methods on extracellular matrix derived hydrogels. Sci Rep 2019;9:14933 https://doi.org/. doi:10.1038/s41598-019-49575-2.
[40] Londono R, Badylak SF. Biologic scaffolds for regenerative medicine: mechanisms of in vivo remodeling. Ann Biomed Eng 2015;43:577–92 https://doi.org/. doi:10.1007/s10439-014-1103-8.
[41] Guyette JP, Charest JM, Mills RW, Jank BJ, Moser PT, Gilpin SE, et al. Bioengineering human myocardium on native extracellular matrix. Circ Res 2016;118:56–72 https://doi.org/. doi:10.1161/CIRCRESAHA.115.306874.
[42] Garreta E, de Oñate L, Fernández-Santos ME, Oria R, Tarantino C, Climent AM, et al. Myocardial commitment from human pluripotent stem cells: rapid production of human heart grafts. Biomaterials 2016;98:64–78 https://doi.org/. doi:10.1016/j.biomaterials.2016.04.003.
[43] Hambor JE. Bioreactor design and bioprocess controls for industrialized cell processing: bioengineering strategies and platform technologies. Bioprocess Int 2012;10:22–33.
[44] Massai D, Isu G, Madeddu D, Cerino G, Falco A, Frati C, et al. A versatile bioreactor for dynamic suspension cell culture. Application to the culture of cancer cell spheroids. PLoS ONE 2016;11:1–16 https://doi.org/. doi:10.1371/journal.pone.0154610.
[45] Isu G, Morbiducci U, De Nisco G, Kropp C, Marsano A, Deriu MA, et al. Modeling methodology for defining a priori the hydrodynamics of a dynamic suspension bioreactor. Application to human induced pluripotent stem cell culture. J Biomech 2019;94:99–106 https://doi.org/. doi:10.1016/j.jbiomech.2019.07.021.
[46] Consolo F, Fiore GB, Truscello S, Caronna M, Morbiducci U, Montevecchi FM, Redaelli A. A computational model for the optimization of transport phenomena in a rotating hollow-fiber bioreactor for artificial liver. Tissue Eng Part C 2009;15:41–55 https://doi:. doi:10.1089/ten.tec.2008.0213.
[47] Consolo F, Bariani C, Mantalaris A, Montevecchi F, Redaelli A, Morbiducci U. Computational modeling for the optimization of a cardiogenic 3D bioprocess of encapsulated embryonic stem cells. Biomech and Model Mechanobiol 2012;11:261–77 https://doi:. doi:10.1007/s10237-011-0308-0.
[48] Sego TJ, Prideaux M, Sterner J, McCarthy BP, Li P, Bonewald LF, et al. Computational fluid dynamic analysis of bioprinted self-supporting perfused tissue models. Biotechnol and Bioeng 2020;117:798–815 https://doi.org/. doi:10.1002/bit.27238.
[49] Bernard M, Jubeli E, Pungente MD, Yagoubi N. Biocompatibility of polymer-based biomaterials and medical devices - regulations, in vitro screening and risk-management. Biomater Sci 2018;6:2025–53 https://doi.org/. doi:10.1039/c8bm00518d.
[50] Özel T, Bártolo PJ, Ceretti E, De Ciurana Gay J, Rodriguez CA, Da Silva JVL. Biomedical devices: design, prototyping, and manufacturing. Wiley; 2016.
[51] Pennella F, Cerino G, Massai D, Gallo D, Falvo D'Urso Labate G, Schiavi A, et al. A survey of methods for the evaluation of tissue engineering scaffold permeability. Ann Biomed Eng 2013;41:2027–41 https://doi.org/. doi:10.1007/s10439-013-0815-5.
[52] Massai D, Pennella F, Gentile P, Gallo D, Ciardelli G, Bignardi C, et al. Image-based three-dimensional analysis to characterize the texture of porous scaffolds. Biomed Res Int 2014;2014:161437 https://doi.org/. doi:10.1155/2014/161437.
[53] Launder BE, Spalding DB. Lectures in mathematical models of turbulence. London, New York: Academic Press; 1972.